

Online Mutual Adaptation of Deep Depth Prediction and Visual SLAM

Shing Yan Loo^{1,2}, Moein Shakeri¹, Sai Hong Tang², Syamsiah Mashohor² and Hong Zhang¹

Abstract—The ability of accurate depth prediction by a convolutional neural network (CNN) is a major challenge for its wide use in practical visual simultaneous localization and mapping (SLAM) applications, such as enhanced camera tracking and dense mapping. This paper is set out to answer the following question: Can we tune a depth prediction CNN with the help of a visual SLAM algorithm even if the CNN is not trained for the current operating environment in order to benefit the SLAM performance? To this end, we propose a novel online adaptation framework consisting of two complementary processes: a SLAM algorithm that is used to generate keyframes to fine-tune the depth prediction and another algorithm that uses the online adapted depth to improve map quality. Once the potential noisy map points are removed, we perform global photometric bundle adjustment (BA) to improve the overall SLAM performance. Experimental results on both benchmark datasets and a real robot in our own experimental environments show that our proposed method improves the overall SLAM accuracy. While regularization has been shown to be effective in multi-task classification problems, we present experimental results and an ablation study to show the effectiveness of regularization in preventing *catastrophic forgetting* in the online adaptation of depth prediction, a single-task regression problem. In addition, we compare our online adaptation framework against the state-of-the-art pre-trained depth prediction CNNs to show that our online adapted depth prediction CNN outperforms the depth prediction CNNs that have been trained on a large collection of datasets.

I. INTRODUCTION

Long-term adaptation in robotics is challenging yet invaluable for many practical applications, ranging from safe autonomous driving to human-robot interaction. This paper is concerned with two related but distinct problems: visual SLAM and single-image depth prediction. Visual SLAM is a problem concerning estimating the structure and camera motion, whereby the camera is attached to a mobile robot or device. On the other hand, single-image depth prediction is a method of predicting a depth map from an image. In particular, we investigate the problem of visual SLAM with online adaptation by on-demand fine-tuning of a depth prediction convolutional neural network (CNN) and integrating online adapted depth prediction to improve structure and motion estimation.

Given a pre-trained depth prediction CNN—which may not necessarily perform well in a real-world setting—can we still

integrate the CNN in a traditional SLAM pipeline such that the depth prediction CNN and the SLAM performance are simultaneously improved? To address this problem, we propose an on-demand adaptation framework. That is, we perform SLAM in an environment whose keyframes are used to determine the *quality* of predicted depth and, depending on the *quality*, we switch between fine-tuning of the depth prediction CNN and incorporating fine-tuned depth prediction into global BA to improve SLAM accuracy. The main contributions of our work are as follows:

- We propose a novel online adaptation framework to fine-tune monocular depth prediction on-demand and perform global BA to improve SLAM accuracy. Experimental results in real-world settings demonstrate an improvement in SLAM accuracy after incorporating online adapted depth in global photometric BA.
- To perform online adaptation without *catastrophic forgetting*, we investigate the effectiveness of EWC regularization in the online adaptation of a depth prediction CNN, a single-task regression problem, as opposed to heavily studied regularization in multi-task classification problems [1], [2]. Experimental results show that use of CNN parameter importance regularization retains the previously learned knowledge better than using only *experience replay* [3]–[5].
- To improve the SLAM accuracy using the adapted depth prediction CNN, we propose using online adapted depth for culling the potential noisy map points before performing global photometric BA, resulting in an improvement in camera tracking and map reconstruction.

II. RELATED WORK

A modern SLAM algorithm [6] typically consists of a front-end and a back-end. Particularly in visual SLAM, the front-end extracts and matches reliable and repeatable features in the images captured by a camera. Two dominant approaches used in the front-end are indirect [7], [8] and direct methods [9], [10] whose goal is to define the observation, odometry and optionally loop constraints for the back-end optimization. Indirect methods preprocess images to generate intermediate feature representation such as handcrafted ORB [11] and deep CNN descriptors [12]–[14] to facilitate feature matching. Alternatively, direct methods operate directly on the raw sensory data—the image pixels—for establishing constraints. Then, the back-end performs a *maximum a posteriori* (MAP), e.g., BA [15] and pose-graph optimization [16], on the established

¹The authors are with Department of Computing Science, University of Alberta, Canada.

²The authors are with Faculty of Engineering, Universiti Putra Malaysia, Malaysia.

Manuscript received April 19, 2021; revised August 16, 2021.

constraints to obtain optimized SLAM variables consisting of a set of camera poses and the position of 3D points obtained from the matched visual features.

Relevantly, we also review background literature on single-image depth prediction. Predicting depth from a single image has shown tremendous progress recently with CNNs. The three main pillars that drive depth prediction accuracy are improved training methods, novel CNN architectures and rich and diverse training datasets. One of the pioneering works is the supervised learning of global and local depth information with a CNN proposed by Eigen et al., which requires ground truth labels to train the CNN parameters. Another seminal research direction is unsupervised learning using photometric reconstruction loss from binocular [17], [18] and motion stereo [19] to overcome the need for ground truth depth. For improved training accuracy, semi-supervised learning incorporates photometric reconstruction and ground truth depth losses [20]. Recently, novel CNN architectures have been proposed to improve depth prediction accuracy, including discretization of the depth output [21], [22], 3D packing and unpacking convolutional blocks [23], dense prediction transformers [24] and generative adversarial networks [25]. Furthermore, single-image relative depth prediction, such as MiDaS [26] and DiverseDepth [27], has been shown to predict accurate relative depth on diverse scene types by leveraging an extensive collection of training datasets.

To overcome the domain gap of single-image depth prediction, online learning has been used to fine-tune a depth prediction CNN on the images available in the target domain. These images typically arrive sequentially [3], [4], [28]. One particular challenge for online fine-tuning is ensuring that learning does not overfit the most *recent* data, a problem known as *catastrophic forgetting* [29]. *Experience replay* has been proposed to mitigate *catastrophic forgetting* by inserting randomly sampled past training data into the current training batch [3]–[5]. An alternative solution is to regularize and preserve the CNN parameters that are important to the previously learned tasks [29], [30]. In a typical multi-task learning scenario, the importance of the CNN parameters can be measured by the magnitude of the gradients with respect to the loss function or output function through the training on a task [30]–[33], which intuitively determines how a perturbation in a CNN parameter affects the loss. Instead of measuring the parameter importance after learning a task and regularizing the parameters in learning the next task, Maltoni and Lomonaco [33] propose single-incremental-task (SIT) learning, which seeks to estimate and consolidate the parameter importance from batch to batch using synaptic intelligence (SI), so that the previously learned knowledge is retained throughout the learning. Unlike SIT, which has to deal with learning new instances or classes, we consider single-task learning whose goal is to preserve the previously learned depth from batch to batch by consolidating the parameter importance using a semi-supervised loss, instead of solving classification problems with ground truth labels [33].

Depth prediction by a CNN has been widely used to benefit SLAM algorithms. A SLAM pipeline can be enhanced by improving feature matching [34] and photometric re-projection

accuracies [35] through the use of depth prediction by CNNs. However, the predicted depth has to be accurate to achieve good performance, an assumption that is often violated in practical robotics applications. Therefore, instead of directly incorporating the predicted depth information into front-end tracking and mapping [34], [35], we design a VO pipeline that only incorporates online adapted depth information in optimizing the structure and motion estimation. To this end, we use two common procedures in SLAM optimization: map point culling and global BA. Removing noisy map points is an essential part of sparse SLAM for preventing erroneous state estimation from being included in optimization (see ORB-SLAM3 [8] and DSO [9]); on the other hand, global photometric BA [36], [37] has been shown to improve SLAM performance further. Assuming that online fine-tuning can obtain reasonable depth prediction (without extreme accuracy), we use depth prediction as a hint to cull the potential noisy map points from being included in global photometric BA, resulting in an improved SLAM accuracy. As for SLAM, we opt for SVO [10] for being a computationally lightweight on an embedded computer, compared to the other state-of-the-art sparse SLAM algorithms [8], [9].

III. METHOD

In this section, we outline our proposed online adaptation framework (see Figure 1). The framework consists of SLAM (Section III-A), online CNN depth adaptation (Section III-B), and global BA with adapted CNN depth (Section III-C).

A. SLAM

We use SVO 2.0 [10] (its monocular variant with edgelets¹) to generate a set of keyframes from a monocular image stream captured by the camera on a mobile robot. Associated with each keyframe are an image, a camera pose, and a set of sparse map points. While the keyframes are being generated, we publish two serialized channels² over a local network containing the newly created keyframes (image, pose and map points) and keyframe graph (latest optimized camera poses and map points of all keyframes). The reason for publishing the keyframe graph is that BA, in most cases, improves the camera pose and map point estimations. Therefore, it is beneficial for improving the training loss in the online adaptation.

B. Online CNN depth adaptation

Our online adaptation is inspired by *early stopping*³ [38], whose goal is to avoid overfitting by stopping the fine-tuning when depth prediction is reasonably accurate, evaluated in terms of validation error (see Algorithm 1 for detailed steps). To this end, we validate the depth prediction accuracy once every m incoming keyframes to determine if the fine-tuning has converged. After determining the stopping criterion, we describe the training details of the online adaptation algorithm.

¹https://github.com/HeYijia/svo_edgelet

²The keyframes are converted to ROS messages before they are published. See <http://wiki.ros.org/msg> for more information.

³https://www.tensorflow.org/api_docs/python/tf/keras/callbacks/EarlyStopping

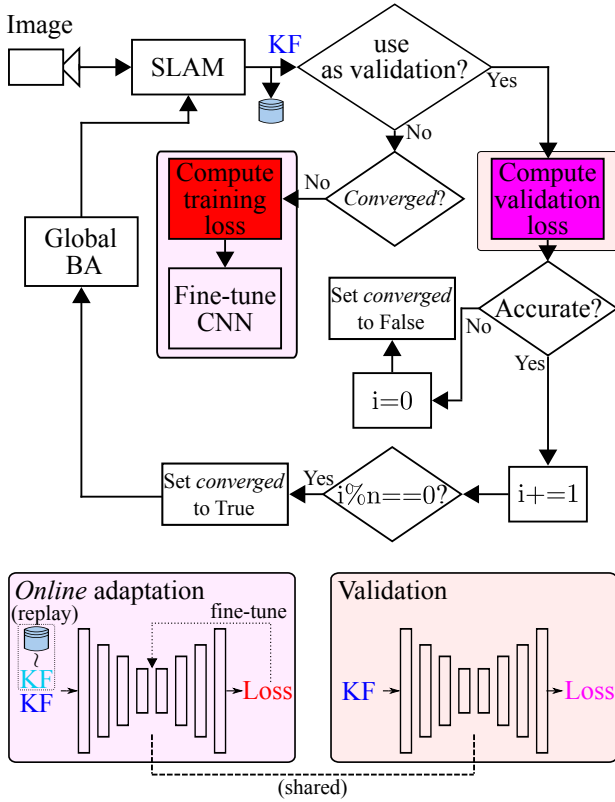


Fig. 1: Our proposed online adaptation framework. We use a SLAM algorithm to generate a sequence of keyframes. The keyframes are classified as training or validation to fine-tune a depth prediction CNN and monitor the adaptation progress. If the training is not converged, we use the most recent keyframe and one randomly sampled old keyframe to fine-tune the CNN. Meanwhile, we calculate the validation loss once every m keyframes to determine if the predicted depth maps are accurate and keep track of the number of continuous accurate depth predictions. If the CNN has been accurate for the past n keyframes, we perform global photometric BA. KF: keyframe.

To adapt a depth prediction CNN on sequential data without *forgetting*, we improve upon the *experience replay* method (i.e., incorporating *recent* data and randomly selecting *old* data into the training batches [3]–[5]) by adding regularization. Training regularization requires the consideration of the learning of two separate tasks \mathcal{T}_1 (learn from *old* data) and \mathcal{T}_2 (learn from *recent* data). The goal is to maximize the training accuracy on both \mathcal{T}_1 and \mathcal{T}_2 , ensuring that we preserve the depth prediction accuracy in the new environment. To reinforce the previously learned knowledge, we modify EWC [30] regularization in the following ways. First, instead of multi-task learning consolidation, we consolidate the importance of the parameters at each training batch and use it in the next batch, which considers the adaptation progress thus far to be absorbed into the posterior probability, i.e., the importance, of the parameters. Second, to estimate the posterior probability, we compute the gradient of the negative log-likelihood of the training loss, assuming constant observation noise for the

Algorithm 1 online adaptation framework represented in a finite-state machine

```

state = IDLE
t = 0
n_converged = 0
m = 5           ▷ Validate every m steps
n = 3           ▷ patience in the context of early stopping
τ_val = 0.2     ▷ Validation error threshold
while not quit do
    if state == IDLE then
        run_global_ba = false
    if t > 0 and t % m == 0 then
        Compute validation error (L_val)
        if L_val < τ_val then
            n_converged += 1
        else
            n_converged = 0
        end if
    end if
    if n_converged > 0 and n_converged % n == 0 then
        run_global_ba = true
    end if
end if
else
    state = FINE_TUNE
end if
else if state == FINE_TUNE then
    Fine-tune the depth prediction CNN
    state = IDLE
end if
end if
if run_global_ba then
    go through all keyframe and publish the keyframe
    depth maps to trigger BA in SVO
end if
t += 1
end while
    
```

input⁴ [39], [40]. Let θ^* be the CNN parameters fine-tuned on the last training batch and θ be the current CNN parameters. We introduce an additional regularization term to the training loss⁵ [30]:

$$\mathcal{L}_{\text{EWC}} = \mathcal{L}_{\text{train}} + \sum_i \frac{\beta}{2} \hat{\mathbf{F}}_i (\theta_i - \theta_i^*)^2 \quad (1)$$

with

$$\begin{aligned} \mathbf{F} &= \mathbf{F} + \mathbf{F}^{(j)} \\ \hat{\mathbf{F}} &= \max\left(\frac{\mathbf{F}}{j}, \max_{\mathbf{F}}\right), \end{aligned} \quad (2)$$

where j is the number of trained batches and \mathbf{F} the consolidated empirical Fisher information matrix at the end of every training batch. $\hat{\mathbf{F}}_i$ is importance of the i -th parameter, which is obtained from the averaged parameter importance

⁴Realistically, observation noise can occur in the violation of brightness constancy assumption and motion blur. This issue can be mitigated by incorporating the heteroscedastic aleatoric uncertainty in training (studied in [39], [40]) and modifying a pre-trained depth prediction CNN to predict an additional uncertainty output.

⁵We explain the details in Appendix A.

matrix $\hat{\mathbf{F}}$ to ensure the preservation of the previously learned knowledge. The empirical Fisher information matrix converges to the Fisher information matrix as more training samples are incorporated [41]. $\max_{\mathbf{F}}$ determines the maximum value of $\hat{\mathbf{F}}$.

Algorithm 2 Online fine-tuning with parameter importance regularization

- 1: Init θ from a pre-trained depth prediction CNN
- 2: $\hat{\mathbf{F}} = 0$ ▷ parameter importance matrix
- 3: **while** not done **do**
- 4: $\theta_{\text{cpy}} = \theta$ ▷ Make a copy
- 5: Get latest keyframe \mathcal{K}_i from SVO
- 6: Train the CNN on \mathcal{K}_i and $\mathcal{K}_{j \sim \{0, \dots, (i-1)\}}$ with \mathcal{L}_{EWC} (see Eq. 1) according to θ and $\hat{\mathbf{F}}$
- 7: Consolidate the parameter importance matrix $\hat{\mathbf{F}}$ according to θ_{cpy} and θ (see Eq. 2)
- 8: **end while**

To compute the training loss ($\mathcal{L}_{\text{train}}$), we use a *semi-supervised* training loss [20], [42], which consists of photometric re-projection ($\mathcal{L}_{\text{photo}}$), sparse depth ($\mathcal{L}_{\text{sparse_depth}}$) and smoothness loss ($\mathcal{L}_{\text{smooth}}$) terms, to be defined below.

First, the photometric reprojection error $\mathcal{L}_{\text{photo}}$ is given by:

$$\mathcal{L}_{\text{photo}} = \frac{1}{|\Omega|} \sum_{\mathbf{p} \in \Omega_s} \min_s pe(I_i, I_{s \rightarrow i}, \mathbf{p}), \text{ and} \quad (3)$$

$$pe(I_i, I_{s \rightarrow i}, \mathbf{p}) = \frac{\alpha}{2} \left(1 - \text{SSIM}(I_i, I_{s \rightarrow i})(\mathbf{p}) \right) + (1 - \alpha) \| I_i(\mathbf{p}) - I_{s \rightarrow i}(\mathbf{p}) \|_1, \quad (4)$$

where $pe(\cdot, \cdot, \cdot)$ is the minimum per-pixel photometric re-projection error [42] between the reconstructed images from the adjacent keyframes $s \in \{i-1, i+1\}$ and the i -th keyframe. To reconstruct the target image from an adjacent image $I_{s \rightarrow i}$, we use bilinear sampling at the valid (Ω_s) re-projected pixel locations \mathbf{p}' using depth prediction $D_{i, \text{CNN}}$, a known camera intrinsics \mathbf{K} and relative keyframe pose transformation $\mathbf{T}_{i \rightarrow s}$ from SVO:

$$\begin{aligned} I_{s \rightarrow i}(\mathbf{p}) &= I_s(\mathbf{p}') \quad \forall \mathbf{p} \in \Omega_s, \\ \mathbf{p}' &\sim \mathbf{K} \mathbf{T}_{i \rightarrow s} D_{i, \text{CNN}}(\mathbf{p}) \mathbf{K}^{-1} \mathbf{p}. \end{aligned} \quad (5)$$

Then, to define $\mathcal{L}_{\text{sparse_depth}}$, we project the sparse map points generated by SVO in each keyframe to form sparse depth maps as *ground truth* labels [20], [43]:

$$\mathcal{L}_{\text{sparse_depth}} = \frac{1}{|\Omega_{i, \text{sparse}}|} \sum_{\mathbf{p} \in \Omega_{i, \text{sparse}}} \left| \frac{1}{D_{i, \text{CNN}}(\mathbf{p})} - \frac{1}{D_{i, \text{sparse}}(\mathbf{p})} \right|, \quad (6)$$

where $D_{i, \text{sparse}}$ is the sparse depth map of keyframe i , $\Omega_{i, \text{sparse}}$ a set of re-projected (sub)pixel locations containing depth values of their corresponding map points from SVO, and $|\Omega_{i, \text{sparse}}|$ the number of valid re-projections. By using inverse depth, near depth is penalized more heavily than far depth.

Finally, we compute the edge-aware smoothness loss $\mathcal{L}_{\text{smooth}}$ using the image gradient:

$$\begin{aligned} \mathcal{L}_{\text{smooth}} &= \frac{1}{N} \sum_{\mathbf{p}} \left(|\partial_x D_{i, \text{CNN}}(\mathbf{p})| e^{-|\partial_x I_i(\mathbf{p})|} \right. \\ &\quad \left. + |\partial_y D_{i, \text{CNN}}(\mathbf{p})| e^{-|\partial_y I_i(\mathbf{p})|} \right) \end{aligned} \quad (7)$$

where ∂ is the gradient operator.

Combining the three loss terms, the final training loss is

$$\mathcal{L}_{\text{train}} = \mathcal{L}_{\text{photo}} + \lambda_1 \mathcal{L}_{\text{sparse_depth}} + \lambda_2 \mathcal{L}_{\text{smooth}} \quad (8)$$

and averaged across the most recent keyframe and a randomly selected old keyframe (*experience replay*). λ_1 and λ_2 are the weighting parameters. Algorithm 2 details the steps involved in the online fine-tuning. To validate the training accuracy, we use the sparse depth loss term:

$$\mathcal{L}_{\text{val}} = \mathcal{L}_{\text{sparse_depth}}. \quad (9)$$

C. Global BA

To optimize the structure and motion, we employ the traditional photometric BA [37], which jointly optimize the keyframe poses and map points. However, we found that the map points generated by SVO, albeit the sparsest amongst the state-of-the-art visual SLAM algorithms [8], [9], still contain noisy and redundant map points. Therefore, with the learned depth information, we introduce a map point culling step before performing global photometric BA. To determine if a map point should be culled, we identify a host keyframe for the map point (see Figure 2) and check if the depth of the map point is within the *correctness* range:

$$g(d_{\text{mp}}, d_{\text{CNN}}) = \begin{cases} 1, & \text{if } |d_{\text{mp}} - d_{\text{CNN}}| < \gamma d_{\text{CNN}} \text{ or} \\ & d_{\text{CNN}} > d_{\text{max}} \\ 0, & \text{otherwise} \end{cases} \quad (10)$$

where d_{CNN} and d_{mp} are the predicted CNN depth and the depth of the map point in the host keyframe, d_{max} a threshold that defines an *effective* depth range of the CNN depth values (similar to a depth sensor) to avoid far map points from being culled prematurely. $g(\cdot)$ evaluates if the map point is valid. Then, we use the standard photometric BA formulation [37] to globally optimize the structure and camera poses (collectively defined as the SLAM variables \mathcal{X}) given by:

$$\mathcal{X}^* = \arg \min_{\mathcal{X}} \frac{1}{2} \sum_k \| \mathbf{e}_k \|_2^2 \quad (11)$$

with

$$\mathbf{e}_k = \mathbf{z}_k - h_k(\mathcal{X}_k) \quad (12)$$

where \mathbf{e}_k is the photometric error induced by a subset of the SLAM variables $\mathcal{X}_k \subseteq \mathcal{X}$, \mathbf{z}_k the reference image patch and $h_k(\cdot)$ the measurement model to obtain the re-projected image patch.

IV. EVALUATION

To evaluate the performance of our proposed method for online CNN adaptation experimentally, our mobile robot hardware setup consists of the following main components: a TurtleBot, an Nvidia Jetson AGX Xavier, an Orbbec Astra RGBD camera, and a laptop⁶, as shown in Figure 3. With the Jetson and laptop connected to the same wireless network, we run the SLAM process (tracking, mapping, and BA) on the Jetson and the fine-tuning process on the laptop.

⁶Specifications: Intel 7820HK CPU and Nvidia GTX 1070 GPU

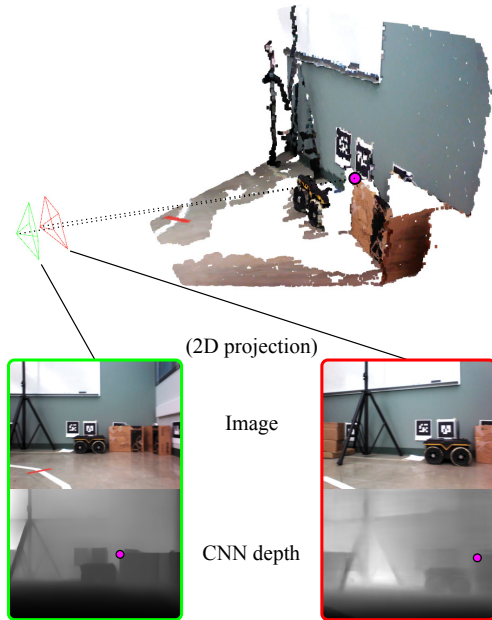


Fig. 2: Assuming the magenta map point is observed in two keyframes (the red and green camera frustums), a host keyframe is selected based on the validation loss (\mathcal{L}_{val}) of the predicted CNN depth, and in this case, the green keyframe has a lower \mathcal{L}_{val} and hence is being selected as the host keyframe of the magenta map point.

To illustrate the effectiveness of the online adaptation, we use Monodepth2’s `mono+stereo_640x192` pre-trained CNN model, which has been trained on outdoor scenes fine-tuned in an indoor environment. For the network to learn, we use Adam optimizer with a learning rate of 10^{-3} , and set the weighting of the loss function λ_1 , λ_2 , α and β at 0.1, 0.1, 0.85 and 5×10^7 , respectively. For EWC consolidation of parameter importance matrix, \max_F is set to 0.001.

In SVO, the main change we made is the increased number of tracked features in the keyframes. We have modified the following parameter values: $\max_{\text{fts}} = 500$, $\text{grid_size} = 20$, and $\text{core_kfs} = 5$. For performing map point culling, we define the *correctness* range by setting $\gamma = 0.5$ and $d_{\text{max}} = 1.5$. This particular design allows for more map points to be generated for fine-tuning the depth prediction CNN. The online adapted depth is then used for removing the potential noisy map points. After the noisy point removal, each map point has a maximum of five photometric re-projections to the nearby keyframes, including the existing 3D-2D constraints (i.e., the list of observed keyframes for the map point), for performing global photometric BA in a separate thread. For each re-projection edge, we get a 3×3 image patch around the re-projected image coordinates to compute the photometric errors.

In the following, we present experimental results to validate the performance of our proposed method. Section IV-A details the dataset that we collect in our laboratory and its purposes. Section IV-B compares and contrasts our proposed online adaptation method with regularization against the state-of-the-art methods. Section IV-C conducts an ablation study to compare different online adaptation schemes in overcoming

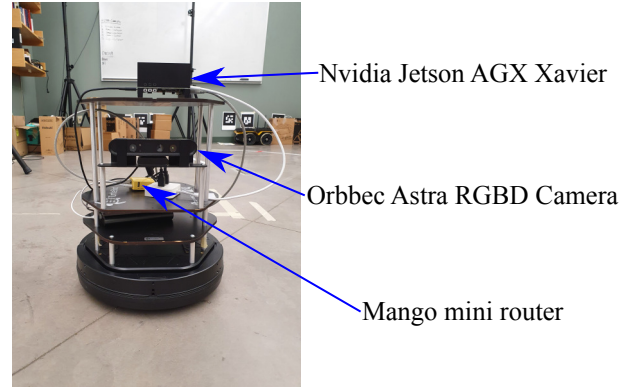


Fig. 3: A TurtleBot equipped with an Nvidia Jetson AGX Xavier and an Orbbec Astra RGBD camera. A Mango mini router is used to create a local wireless network to communicate between the Jetson and a laptop.

catastrophic forgetting. Section IV-D presents quantitative and qualitative results of our proposed map point culling with online adapted depth and global photometric BA to improve SLAM accuracy. Section IV-E analyzes the accuracy of online adapted and pre-trained depth prediction to show the advantage of using online adaptation to improve SLAM performance. And lastly, Section IV-F evaluates the runtimes of our proposed online adaptation framework.

A. Laboratory dataset

The reason for collecting our own dataset is that the image sequences in existing benchmarking datasets [44]–[46] are not long enough to evaluate and illustrate the effectiveness of our proposed online adaptation. Our dataset contains two sequences (dubbed `Lab1` and `Lab2`) that we collected in our laboratory (see Figure 5 for the images of the captured environment). We record both sequences in the same environment, with the difference being the `Lab2` sequence (16366 images) is longer than the `Lab1` sequence (10611 images).

B. Online adaptation

To evaluate the effectiveness of our proposed online adaptation, we compare our method against the state-of-the-art methods: a SLAM-based approach by Luo et al. [28] (Section IV-B1) and a learning-based approach by Kuznetsov et al. [4] (Section IV-B2). For the comparison, we adopt the datasets and performance metric in [28]. The datasets are the ICL-NUIM [47] and TUM RGB-D [44] datasets and the performance metric is the percentage of overall depth pixels below 10% relative errors, i.e., $\frac{|D - D_{gt}|}{D_{gt}} < 0.1$.

1) *SLAM-based online adaptation*: Table I compares the overall depth accuracy between our method and a similar method by Luo et al. [28]. Our method improves the overall depth accuracy by around 23% (the last two columns), compared to 4% (2nd and 3rd column) by Luo et al. [28]. The performance gap could be due to the number of keyframes used in the fine-tuning; we use all the keyframes generated by SVO [10], whereas Luo et al. [28] use the keyframe pairs by LSD-SLAM [48] that have a dominant horizontal

TABLE I: A comparison between the overall depth accuracy of our method and Luo et al.’s [28] SLAM-based online adaptation on the ICL-NUIM [47] and TUM RGB-D [44] datasets. (TUM/seq1: fr3_long_office_household, TUM/seq2: fr3_nostructure_texture_near_withloop, TUM/seq3: fr3_structure_texture_far)

Sequence	Percentage of correct depth (%)			
	Pre-trained [28]	[28]	Pre-trained*	Ours*
ICL/office0	19.117	22.206	8.766	12.541
ICL/office1	28.086	31.289	19.739	21.870
ICL/office2	21.695	21.695	4.591	42.244
ICL/living0	18.680	23.278	7.726	41.375
ICL/living1	21.071	22.774	8.518	49.075
ICL/living2	16.150	20.995	13.509	25.159
TUM/seq1	18.208	20.259	10.999	23.861
TUM/seq2	25.796	29.014	12.678	52.162
TUM/seq3	20.668	30.156	10.295	37.848
Average	21.052	24.630	10.758	34.015

* Scaled to ground truth depth

motion as simulated static stereo pairs. Besides, Luo et al. [28] perform online adaptation using most *recent* keyframes only, which performs the worst in the online adaptation scheme comparison (see Section IV-C). Note that Luo et al. [28] evaluate the keyframe depth accuracy based on the fine-tuned CNN models in different fine-tuning stages, which may result in different overall depth correctness should the final fine-tuned CNN model be used in the evaluation.

2) *Learning-based online adaptation:* Table II compares our method against a learning-based online adaptation method, CoMoDa⁷ [4]. Overall, our proposed SLAM-based method outperforms CoMoDa by around 5% (the last two columns). One particular challenge in end-to-end online adaptation is the simultaneous fine-tuning of depth and pose prediction CNNs, and the pose prediction CNN is not trained in the tested indoor environments; on the contrary, we obtain camera poses from SVO [10]. Furthermore, accurate camera pose estimation is essential when performing online adaptation (see Equation 5). Plus, CoMoDa does not use regularization in online adaptation, which is a reason that it performs worse than our method (see Section IV-C).

C. Learning against catastrophic forgetting in online adaptation

To evaluate the effectiveness of our proposed regularization in online adaptation, we perform an ablation study to measure the impact of different adaptation schemes on alleviating *catastrophic forgetting*. To this end, we examine the overall depth accuracy (using the same 10% relative error as the metric) on the ICL-NUIM [47] and TUM RGB-D [44] datasets.

Table III shows that performing online adaptation using only most *recent* keyframes has the worst overall depth accuracy (3rd column), compared to using the most *recent* keyframe with *experience replay* and regularization (the last two columns). Moreover, Figure 4 illustrates *catastrophic forgetting* on the lr_kt1 sequence, where the CNN is overfitted to the most *recent* keyframes in the sequence. In general, a combination of *experience replay* and regularization in online

TABLE II: A comparison between the overall depth accuracy of our method and CoMoDa’s [4] end-to-end online adaptation on the ICL-NUIM [47] and TUM RGB-D [44] datasets. Both our method and CoMoDa [4] are fine-tuned on the same pre-trained CNN model, mono+stereo_640x192 [42]. (TUM/seq1: fr3_long_office_household, TUM/seq2: fr3_nostructure_texture_near_withloop, TUM/seq3: fr3_structure_texture_far)

Sequence	Percentage of correct depth (%)		
	Pre-trained*	Ours*	CoMoDa* [4]
ICL/office0	13.660	32.98	21.054
ICL/office1	22.453	38.383	41.623
ICL/office2	22.514	44.790	37.374
ICL/living0	17.659	48.158	35.164
ICL/living1	22.585	51.531	46.148
ICL/living2	21.606	35.757	35.571
TUM/seq1	16.931	27.915	33.120
TUM/seq2	17.722	41.782	33.708
TUM/seq3	23.026	50.339	39.769
Average	19.795	41.293	35.948

*Median scaling to ground truth depth

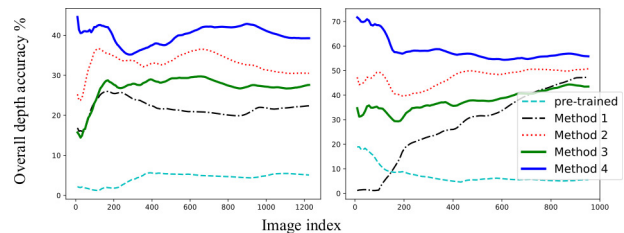


Fig. 4: A comparison of different online adaptation schemes tested on the ICL-NUIM [47] of_kt3 (left) and lr_kt1 (right) using the final online adapted CNN. Adaptation accuracy is measured by the averaged percentage of overall depth accuracy over all frames up to the frame. Method 1: fine-tuning on most *recent* keyframes only; Method 2: fine-tuning on the most *recent* keyframe with *experience replay*; Method 3: fine-tuning on the most *recent* keyframe with regularization; Method 4: fine-tuning on the most *recent* keyframe with *experience replay* and regularization.

adaptation has the best overall depth accuracy (see the last column in Table III and Figure 4). Thus, it validates the effectiveness of our proposed online adaptation scheme. However, for a short sequence, regularization can inhibit changes in the CNN parameters and hurt the online adaptation accuracy (2nd last row in Table III). For the sake of completeness, we compare the online adaptation performances using the three popular regularization techniques⁹: EWC [30], MAS [31] and SI [32], and they perform similarly.

D. Effect of global photometric BA with map point culling on SLAM accuracy

After the depth prediction CNN has been fine-tuned to a reasonable accuracy, our following proposed method incorporates the online adapted depth into removing potential noisy map points and then performs photometric global BA to improve SLAM performance.

1) *Camera tracking error:* To measure the camera tracking performance, we use the standard absolute trajectory RMSE

⁹See Appendix B for more information. The regularization strength (λ) in Eq. 19) for SI and MAS are set to 1.0 and 0.5, respectively.

⁷We generate results using CoMoDa’s [4] open-source code⁸

TABLE III: An ablation study on different online adaptation schemes using our proposed framework on the ICL-NUM [47] and TUM RGB-D [44] datasets. (TUM/seq1: fr3_long_office_household, TUM/seq2: fr3_nostructure_texture_near_withloop, TUM/seq3: fr3_structure_texture_far)

Sequence	Percentage of correct depth (%)			
	Pre-trained	Ours(a)	Ours(b)	Ours(c)
ICL/office0	8.766	7.249	12.734	12.541
ICL/office1	19.739	4.034	22.613	21.870
ICL/office2	4.591	21.449	34.609	42.244
ICL/living0	7.726	13.179	22.883	41.375
ICL/living1	8.518	38.246	41.149	49.075
ICL/living2	13.509	9.110	13.117	25.159
TUM/seq1	10.999	16.012	19.782	23.861
TUM/seq2	12.678	14.457	37.539	52.162
TUM/seq3	10.295	49.515	51.545	37.848
Average	10.758	19.250	28.441	34.015

- (a) Online adaptation with two most *recent* keyframes
 (b) Online adaptation with the most *recent* keyframe and *experience replay*
 (c) Online adaptation with the most *recent* keyframe, *experience replay* and regularization

TABLE IV: A comparison of the camera tracking ATEs with and without global photometric BA on the ICL-NUM [47] and TUM RGB-D [44] datasets. (TUM/seq1: fr3_long_office_household, TUM/seq2: fr3_nostructure_texture_near_withloop, TUM/seq3: fr3_structure_texture_far)

Sequence	Without BA*	With BA*
ICL/office0	0.363	0.323
ICL/office1	0.196	0.204
ICL/office2	0.170	0.171
ICL/living0	0.220	0.227
ICL/living1	0.032	0.026
ICL/living2	0.161	0.158
TUM/seq1	0.088	0.073
TUM/seq2	0.029	0.011
TUM/seq3	0.011	0.012
Average	0.141	0.134

*Aligned to ground truth trajectory

(ATE) as the performance metric on the ICL-NUIM [47] and TUM RGB-D [44] datasets, which contains ground truth camera poses for the evaluation. Table IV compares the ATEs obtained from SVO and SVO with our proposed map point culling and global photometric BA. In general, performing global photometric BA leads to a lower overall ATE than that of without the global BA (compare the last two columns in Table IV). Our proposed photometric global BA with map point culling reduces the ATE by more than 50% (from 0.029 to 0.011) on the TUM/seq2 sequence, likely due to the better online adaptation of depth prediction (check the corresponding rows in Table III).

2) *Map reconstruction error:* To highlight the effectiveness of the online adaptation, we evaluate the accuracy of the SVO map on long sequences, Lab1 and Lab2, from our Laboratory dataset. We use the scale-invariant inverse depth error as the performance metric [49] given by:

$$e_{si} = \sqrt{\frac{1}{N} \sum_i d_i^2 - \frac{1}{N^2} (\sum_i d_i)^2} \quad (13)$$

where $d_i = \log z_i - \log z_i^*$, and the superscript * indicates the ground truth depth.

TABLE V: A comparison of the number of points and depth error of the SVO map with and without our proposed map point culling and global photometric BA. A larger `max_fts` generates more map points in SVO.

BA	MP culling	SVO param (<code>max_fts</code>)	Lab1		Lab2	
			No. map points	e_{si}	No. map points	e_{si}
		120	13992	0.533	19856	0.607
✓		120	14469	0.545	20464	0.625
✓	✓	120	7435	0.473	9226	0.495
		500	19179	0.527	25743	0.540
✓		500	19208	0.515	23998	0.528
✓	✓	500	9916	0.493	12686	0.472

Note: `max_fts` is set at 120 by default in SVO.

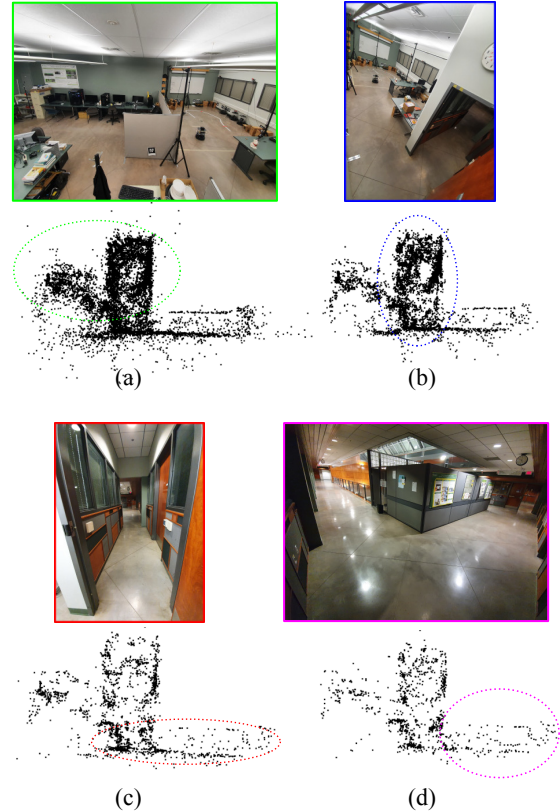


Fig. 5: Qualitative comparisons between different *correctness* thresholds used in map point (MP) culling: (a) no culling, (b) MP culling with $\alpha = 0.5$, (c) MP culling with $\alpha = 0.25$ and (d) MP culling with $\alpha = 0.15$.

To allow for a more accurate online adaptation accuracy, we increase the number of map points by tweaking the `max_fts` parameter in SVO. Table V shows that the SVO map accuracy is improved by our proposed map point culling with online adapted depth prediction and global photometric BA (compare the e_{si} with and without BA in Table V and Figure 5(a) and 5(b)). The improved map accuracy also comes at the expense of removing good map points, which can be mitigated by having a training scheme with better online adaptation performance. As a result, our proposed online adaptation framework achieves a mutual adaptation of depth prediction and visual SLAM.

TABLE VI: A comparison of depth errors of MiDaS [26], DiverseDepth [27] and our online adapted Monodepth2 [42] CNN model.

Method	e_{si}	
	Lab1	Lab2
MiDaS (v2.1)	0.271	0.256
MiDaS (v3.0)	0.315	0.322
DiverseDepth	0.450	0.435
Pre-trained	0.401	0.399
Ours	0.235	0.219

[†] only the re-projected (sub)pixels

E. Online adaptation vs. relative depth prediction

A competing idea to our online adaption for resolving the domain gap in single-image depth prediction is to train a network with a large number of datasets across multiple domains to improve its generalization. Unlike absolute depth prediction, which is trained in a narrow domain, state-of-the-art relative depth prediction CNN models, such as MiDaS [26] and DiverseDepth [27], have been trained on an extensive collection of datasets. Therefore, to compare between online adapted depth and pre-trained depth prediction, we use the same scale-invariant inverse depth error (e_{si}) described in Section IV-D2.

Table VI shows a quantitative comparison of the depth errors of MiDaS, DiverseDepth and our fine-tuned Monodepth2 CNN model. On both sequences (2nd and 3rd column), our method has the lowest depth error in comparison with the relative depth prediction CNNs¹⁰ (MiDaS and DiverseDepth) (see Figure 6 for a qualitative comparison). Due to the similarity between Lab1 and Lab2, the depth prediction errors of MiDaS, DiverseDepth and pre-trained Monodepth2 are similar in both sequences. Conversely, our method can further boost the depth prediction accuracy (see the last row of Table VI) resulting from our proposed online adaptation, especially on the longer sequence (Lab2).

F. Runtime evaluation

The two main time-consuming processes in our proposed online adaptation framework are depth prediction and fine-tuning. On average, depth prediction and one fine-tuning iteration take about 18 ms and 250 ms to process, respectively. Incidentally, the global photometric BA time consumption varies according to the total number of photometric re-projections between the map points and keyframes, but real-time processing should not be affected as the BA process itself runs on another thread.

V. CONCLUSION

In this paper, we have addressed a practical robotics problem concerning the use of single-image depth prediction to improve SLAM performance. Particularly, we have proposed a novel online adaptation framework in which the fine-tuning is enhanced with regularization for retaining the previously learned knowledge while the CNN is being trained continually.

¹⁰For relative depth prediction to achieve maximum accuracy, accurate scale- and shift-correction for each predicted depth map is required [27], [50]

Furthermore, we have investigated the use of regularization in the learning of depth prediction, a single-task regression problem, with quantitative results and an ablation study to show its effectiveness against *catastrophic forgetting*. Also, we have demonstrated the use of fine-tuned depth prediction for map point culling before running global photometric BA, resulting in improved camera tracking and map reconstruction. Lastly, we have compared our online adaptation framework against state-of-the-art depth prediction CNNs that have been trained on a large number of datasets across domains, showing that our online adapted depth prediction CNN has a lower depth error, especially after performing online adaptation on a long sequence.

One main shortcoming is that SVO is a visual odometry system and is prone to drift over time. For long-term adaptation problems, it would be better to incorporate loop closure and establish feature correspondences among the closed-loop keyframes to enhance the map reconstruction accuracy while the CNN is being online adapted. In return, the long-term adapted depth prediction CNN can be used to improve the SLAM accuracy further.

APPENDIX

A. Adapted EWC regularization for single-task regression problem

To perform online adaptation incrementally on a single task, we measure and consolidate the importance of the CNN parameters at each iteration, allowing for the preservation of learned knowledge. The EWC loss comprises the training loss and a regularizer to fine-tune the CNN parameters while preserving the important parameters measured through consolidation.

Formally, let E be the loss function of the problem at hand and assuming E to be locally smooth. we may expand the function about θ_0 using Taylor series approximation:

$$E(\theta) = E(\theta_0) + \mathbf{J}_\theta(\theta_0)(\theta - \theta_0) + \frac{1}{2!}(\theta - \theta_0)^T \mathbf{H}_\theta(\theta_0)(\theta - \theta_0) + \text{h.o.t.}, \quad (14)$$

where $\mathbf{J}_\theta(\theta_0)$ and $\mathbf{H}_\theta(\theta_0)$ are the Jacobian and Hessian of E evaluated at θ_0 , respectively. Assume that the CNN is fine-tuned on *old* data \mathcal{T}_1 , which implies that θ_0 would be at a local minimum (denoted by $\theta_{\mathcal{T}_1}^*$) and that $E'(\theta_{\mathcal{T}_1}^*) = 0$, we can rewrite Equation 14 as

$$E_{\mathcal{T}_1}(\theta) \approx E(\theta_{\mathcal{T}_1}^*) + \frac{1}{2!}(\theta - \theta_{\mathcal{T}_1}^*)^T \mathbf{H}_\theta(\theta_{\mathcal{T}_1}^*)(\theta - \theta_{\mathcal{T}_1}^*) \quad (15)$$

where $E_{\mathcal{T}_1}$ is the approximated error for *old* data \mathcal{T}_1 . Next, to fine-tune the CNN on *recent* data \mathcal{T}_2 , we can use the following loss function:

$$E(\theta) = E_{\mathcal{T}_2}(\theta) + \beta E_{\mathcal{T}_1}(\theta), \quad (16)$$

where β controls the weighting between the two loss terms. Substituting Equation 15 into Equation 16, we get

$$\begin{aligned} E(\theta) &= E_{\mathcal{T}_2}(\theta) + \beta \left(E(\theta_{\mathcal{T}_1}^*) + \frac{1}{2}(\theta - \theta_{\mathcal{T}_1}^*)^T \mathbf{H}_\theta(\theta_{\mathcal{T}_1}^*)(\theta - \theta_{\mathcal{T}_1}^*) \right) \\ &= E_{\mathcal{T}_2}(\theta) + \frac{\beta}{2} \left((\theta - \theta_{\mathcal{T}_1}^*)^T \mathbf{H}_\theta(\theta_{\mathcal{T}_1}^*)(\theta - \theta_{\mathcal{T}_1}^*) \right), \quad (17) \end{aligned}$$



Fig. 6: A qualitative comparison of the back-projected point clouds (shown in black) between (from left to right) ground truth depth with SVO map points (in blue), MiDaS v2.1, MiDaS v3.0, DiverseDepth, pre-trained Monodepth2, and our online adapted Monodepth2. From top to bottom: first and second viewpoint of the back-projected depth maps and the predicted depth maps by the aforementioned CNN models. The predicted depth maps are scaled to ground truth. Best viewed digitally.

in which the first term of Equation 15 is being treated as a constant and can be eliminated in the optimization. To measure the importance of the parameters contained in the Hessian matrix, Kirkpatrick et al. approximate the Gaussian distribution of the posterior with Laplace approximation, whereby diagonal of the Fisher information matrix replaces the Hessian matrix for the approximation of the posterior [30]:

$$E(\theta) = E_{\mathcal{T}_2}(\theta) + \frac{\beta}{2} \left(\sum_i \mathbf{F}_i(\theta_i - \theta_{\mathcal{T}_1, i}^*)^2 \right). \quad (18)$$

B. SI and MAS regularizations

Similar to EWC regularization, SI and MAS can be expressed using the following loss function:

$$\mathcal{L} = \mathcal{L}_{\text{train}} + \lambda \sum_i \Omega_i (\theta_i - \theta_{\mathcal{T}_1, i}^*)^2, \quad (19)$$

with the main difference being the estimation of the weight importance matrix, Ω_i . For MAS, the weight importance matrix is given by the gradient of the squared L_2 -norm of the CNN output function, G [31]:

$$\Omega_i = \frac{1}{N} \sum_{j=1}^N \frac{\partial \|G(x_j; \theta)\|_2^2}{\partial \theta_i}, \quad (20)$$

whereas for SI, the weight importance matrix is given by [32]:

$$\Omega_i = \sum_j \frac{\omega_{ij}}{(\Delta\theta_{ij})^2 + \xi}, \quad (21)$$

where ω_{ij} is the estimated per-parameter contribution to the total loss, and $\Delta\theta_{ij}$ the total trajectory of the parameter.

REFERENCES

- [1] Matthias Delange, Rahaf Aljundi, Marc Masana, Sarah Parisot, Xu Jia, Ales Leonardis, Greg Slabaugh, and Tinne Tuytelaars. A continual learning survey: Defying forgetting in classification tasks. *IEEE transactions on pattern analysis and machine intelligence*, 2021.
- [2] German I Parisi, Ronald Kemker, Jose L Part, Christopher Kanan, and Stefan Wermter. Continual lifelong learning with neural networks: A review. *Neural Networks*, 113:54–71. Elsevier, 2019.
- [3] Milo Knowles, Valentin Peretroukhin, W Nicholas Greene, and Nicholas Roy. Toward robust and efficient online adaptation for deep stereo depth estimation. In *International Conference on Robotics and Automation (ICRA)*, pages 12292–12198, 2021.
- [4] Yevhen Kuznietsov, Marc Proesmans, and Luc Van Gool. Comoda: Continuous monocular depth adaptation using past experiences. In *Proceedings of the IEEE/CVF Winter Conference on Applications of Computer Vision (WACV)*, pages 2907–2917, January 2021.
- [5] Zhenyu Zhang, Stéphane Lathuilière, Elisa Ricci, Nicu Sebe, Yan Yan, and Jian Yang. Online depth learning against forgetting in monocular videos. In *Proceedings of the IEEE/CVF Conference on Computer Vision and Pattern Recognition*, pages 4494–4503, 2020.
- [6] Cesar Cadena, Luca Carlone, Henry Carrillo, Yasir Latif, Davide Scaramuzza, José Neira, Ian Reid, and John J Leonard. Past, present, and future of simultaneous localization and mapping: Toward the robust-perception age. In *IEEE Transactions on robotics*, 32(6):1309–1332, 2016.
- [7] Masashi Yokozuka, Shuji Oishi, Simon Thompson, and Atsuhiko Banno. Vitamin-e: Visual tracking and mapping with extremely dense feature points. In *Proceedings of the IEEE/CVF Conference on Computer Vision and Pattern Recognition*, pages 9641–9650, 2019.
- [8] Carlos Campos, Richard Elvira, Juan J Gómez Rodríguez, José MM Montiel, and Juan D Tardós. Orb-slam3: An accurate open-source library for visual, visual-inertial, and multimap slam. *IEEE Transactions on Robotics*, 2021.
- [9] Jakob Engel, Vladlen Koltun, and Daniel Cremers. Direct sparse odometry. *IEEE transactions on pattern analysis and machine intelligence*, 40(3):611–625, 2017.
- [10] Christian Forster, Zichao Zhang, Michael Gassner, Manuel Werlberger, and Davide Scaramuzza. Svo: Semidirect visual odometry for monocular and multicamera systems. *IEEE Transactions on Robotics*, 33(2):249–265, 2016.
- [11] Ethan Rublee, Vincent Rabaud, Kurt Konolige, and Gary Bradski. ORB: An efficient alternative to SIFT or SURF. In *International Conference on Computer Vision*, pages 2564–2571, 2011.
- [12] Paul-Edouard Sarlin, Cesar Cadena, Roland Siegwart, and Marcin Dymczyk. From coarse to fine: Robust hierarchical localization at large scale. In *Proceedings of the IEEE/CVF Conference on Computer Vision and Pattern Recognition*, pages 12716–12725, 2019.
- [13] Zhuang Dai, Xinghong Huang, Weinan Chen, Li He, and Hong Zhang. A Comparison of CNN-Based and Hand-Crafted Keypoint Descriptors. In *International Conference on Robotics and Automation (ICRA)*, pages 2399–2404, 2019.
- [14] Shenghao Li, Shuang Liu, Qunfei Zhao, and Qiaoyang Xia. Quantized Self-supervised Local Feature for Real-time Robot Indirect VSLAM *IEEE/ASME Transactions on Mechatronics*, 2021.
- [15] Hauke Strasdat, José MM Montiel, and Andrew J Davison. Visual SLAM: why filter? *Image and Vision Computing*, 30(2):65–77. Elsevier, 2012.
- [16] Giorgio Grisetti, Rainer Kümmerle, Cyrill Stachniss, and Wolfram Burgard. A tutorial on graph-based SLAM. *IEEE Intelligent Transportation Systems Magazine*, 2(4):31–43, 2010.
- [17] Ravi Garg, Vijay Kumar Bg, Gustavo Carneiro, and Ian Reid. Unsupervised cnn for single view depth estimation: Geometry to the rescue. In *European conference on computer vision*, pages 740–756. Springer, 2016.
- [18] Clément Godard, Oisín Mac Aodha, and Gabriel J Brostow. Unsupervised Monocular Depth Estimation with Left-Right Consistency. In *Proceedings of the IEEE conference on computer vision and pattern recognition*, pages 270–279, 2017.
- [19] Tinghui Zhou, Brown Matthew, Noah Snavely, and David-G Lowe. Unsupervised learning of depth and ego-motion from video. In *Proceedings of the IEEE conference on computer vision and pattern recognition*, pages 1851–1858, 2017.
- [20] Ali Jahani Amiri, Shing Yan Loo, and Hong Zhang. Semi-supervised monocular depth estimation with left-right consistency using deep neural network. In *2019 IEEE International Conference on Robotics and Biomimetics (ROBIO)*, pages 602–607. IEEE, 2019.
- [21] Huan Fu, Mingming Gong, Chaohui Wang, Kayhan Batmanghelich, and Dacheng Tao. Deep ordinal regression network for monocular depth estimation. In *Proceedings of the IEEE conference on computer vision and pattern recognition*, pages 2002–2011, 2018.
- [22] Shariq Farooq Bhat, Ibraheem Alhashim, and Peter Wonka. Adabins: Depth estimation using adaptive bins. In *Proceedings of the IEEE conference on computer vision and pattern recognition*, pages 4009–4018, 2021.
- [23] Vitor Guizilini, Rares Ambrus, Sudeep Pillai, Allan Raventos, and Adrien Gaidon. 3d packing for self-supervised monocular depth estimation. In *Proceedings of the IEEE conference on computer vision and pattern recognition*, pages 2485–2494, 2020.
- [24] René Ranftl, Alexey Bochkovskiy, and Vladlen Koltun. Vision transformers for dense prediction. In *Proceedings of the IEEE/CVF International Conference on Computer Vision*, pages 12179–12188, 2021.
- [25] Filippo Aleotti, Fabio TOSi, Matteo Poggi, and Stefano Mattoccia. Generative adversarial networks for unsupervised monocular depth prediction. In *Proceedings of the European Conference on Computer Vision (ECCV) Workshops*, 2018.
- [26] René Ranftl, Katrin Lasinger, David Hafner, Konrad Schindler, and Vladlen Koltun. Towards robust monocular depth estimation: Mixing datasets for zero-shot cross-dataset transfer. *arXiv preprint arXiv:1907.01341*, 2019.
- [27] Wei Yin, Xinlong Wang, Chunhua Shen, Yifan Liu, Zhi Tian, Songcen Xu, Changming Sun, and Dou Renyin. Diversedepth: Affine-invariant depth prediction using diverse data. *arXiv preprint arXiv:2002.00569*, 2020.
- [28] Hongcheng Luo, Yang Gao, Yuhao Wu, Chunyuan Liao, Xin Yang, and Kwang-Ting Cheng. Real-time dense monocular slam with online adapted depth prediction network. *IEEE Transactions on Multimedia*, 21(2):470–483, 2018.
- [29] German I Parisi, Ronald Kemker, Jose L Part, Christopher Kanan, and Stefan Wermter. Continual lifelong learning with neural networks: A review. *Neural Networks*, 113:54–71, 2019.
- [30] James Kirkpatrick, Razvan Pascanu, Neil Rabinowitz, Joel Veness, Guillaume Desjardins, Andrei A Rusu, Kieran Milan, John Quan, Tiago Ramalho, Agnieszka Grabska-Barwinska, et al. Overcoming catastrophic

forgetting in neural networks. *Proceedings of the national academy of sciences*, 114(13):3521–3526, 2017.

- [31] Rahaf Aljundi, Francesca Babiloni, Mohamed Elhoseiny, Marcus Rohrbach, and Tinne Tuytelaars. Memory aware synapses: Learning what (not) to forget. In *Proceedings of the European Conference on Computer Vision (ECCV)*, pages 139–154, 2018.
- [32] Friedemann Zenke, Ben Poole, and Surya Ganguli. Continual learning through synaptic intelligence. In *International Conference on Machine Learning*, pages 3987–3995. PMLR, 2017.
- [33] Davide Maltoni and Vincenzo Lomonaco. Continuous learning in single-incremental-task scenarios. *Neural Networks*, 116:56–73, 2019.
- [34] Shing Yan Loo, Ali Jahani Amiri, Syamsiah Mashohor, Sai Hong Tang, and Hong Zhang. Cnn-svo: Improving the mapping in semi-direct visual odometry using single-image depth prediction. In *2019 International Conference on Robotics and Automation (ICRA)*, pages 5218–5223. IEEE, 2019.
- [35] Nan Yang, Rui Wang, Jorg Stuckler, and Daniel Cremers. Deep virtual stereo odometry: Leveraging deep depth prediction for monocular direct sparse odometry. In *Proceedings of the European Conference on Computer Vision (ECCV)*, pages 817–833, 2018.
- [36] Nikolaus Demmel, Maolin Gao, Emanuel Laude, Tao Wu, and Daniel Cremers. Distributed photometric bundle adjustment. In *2020 International Conference on 3D Vision (3DV)*, pages 140–149. IEEE, 2020.
- [37] Hatem Alismail, Brett Browning, and Simon Lucey. Photometric bundle adjustment for vision-based slam. In *Asian Conference on Computer Vision*, pages 324–341. Springer, 2016.
- [38] Lutz Prechelt. Early stopping-but when? In *Neural Networks: Tricks of the trade*, pages 55–69. Springer, 1998.
- [39] Nan Yang, Lukas von Stumberg, Rui Wang, and Daniel Cremers. D3vo: Deep depth, deep pose and deep uncertainty for monocular visual odometry. In *Proceedings of the IEEE/CVF Conference on Computer Vision and Pattern Recognition*, pages 1281–1292, 2020.
- [40] Alex Kendall, and Yarin Gal. What Uncertainties Do We Need in Bayesian Deep Learning for Computer Vision? In *Advances in neural information processing systems*, pages 5574–5584, 2017.
- [41] Limitations of the empirical Fisher approximation for natural gradient descent. In *em Advances in neural information processing systems*, pages 4158–4169, 2019.
- [42] Clément Godard, Oisín Mac Aodha, Michael Firman, and Gabriel J Brostow. Digging into self-supervised monocular depth estimation. In *Proceedings of the IEEE/CVF International Conference on Computer Vision*, pages 3828–3838, 2019.
- [43] Lokender Tiwari, Pan Ji, Quoc-Huy Tran, Bingbing Zhuang, Saket Anand, and Manmohan Chandraker. Pseudo rgb-d for self-improving monocular slam and depth prediction. In *European Conference on Computer Vision*, pages 437–455. Springer, 2020.
- [44] Jürgen Sturm, Nikolas Engelhard, Felix Endres, Wolfram Burgard, and Daniel Cremers. A benchmark for the evaluation of rgb-d slam systems. In *2012 IEEE/RSJ international conference on intelligent robots and systems*, pages 573–580. IEEE, 2012.
- [45] Nathan Silberman, Derek Hoiem, Pushmeet Kohli, and Rob Fergus. Indoor segmentation and support inference from rgb-d images. In *European conference on computer vision*, pages 746–760. Springer, 2012.
- [46] Angela Dai, Angel X Chang, Manolis Savva, Maciej Halber, Thomas Funkhouser, and Matthias Nießner. Scannet: Richly-annotated 3d reconstructions of indoor scenes. In *Proceedings of the IEEE conference on computer vision and pattern recognition*, pages 5828–5839, 2017.
- [47] Ankur Handa, Thomas Whelan, John McDonald, and Andrew J Davison. A benchmark for rgb-d visual odometry, 3d reconstruction and slam. In *2014 IEEE international conference on Robotics and automation (ICRA)*, pages 1524–1531. IEEE, 2014.
- [48] Jakob Engel, Thomas Schöps, and Daniel Cremers. Lsd-slam: Large-scale direct monocular slam. In *European conference on computer vision*, pages 834–849. Springer, 2014.
- [49] B. Ummenhofer, H. Zhou, J. Uhrig, N. Mayer, E. Ilg, A. Dosovitskiy, and T. Brox. Demon: Depth and motion network for learning monocular stereo. In *IEEE Conference on Computer Vision and Pattern Recognition (CVPR)*, 2017.
- [50] Shing Yan Loo, Syamsiah Mashohor, Sai Hong Tang, and Hong Zhang. Deeprelativefusion: Dense monocular slam using single-image relative depth prediction. In *International Conference on Intelligent Robots and Systems (IROS)*. IEEE, 2021.



Shing Yan Loo received his MSc degree from the Universiti Putra Malaysia (UPM). He is currently enrolled on a Dual PhD program offered by UPM and University of Alberta. His research interest lies at the intersection of visual SLAM and deep learning.



Moein Shakeri received the M.S. degree in computer engineering from Ferdowsi University, Iran in 2009, and Ph.D. degree in computing science from University of Alberta, Canada, 2019. During his Ph.D. he has been awarded several grants, and Ph.D outstanding thesis award. He is currently working as post-doctoral research fellow in the department of computing science at the University of Alberta. His research interests include dense map reconstruction, loop closure detection, object detection and segmentation, and polarimetric 3D reconstruction.



S. Mashohor received her B.Eng degree from the Department of Computer and Communication Systems Engineering, Universiti Putra Malaysia (UPM) in 2002. Then, she continued her study for PhD on “Genetic Algorithm based Printed Circuit Board optical inspection” at the Department of Electronics and Electrical Engineering, University of Edinburgh, UK and graduated in 2006. She has been with the Department of Computer and Communication Systems Engineering, UPM as a tutor in 2002, lecturer in 2006, senior lecturer in 2009 until 2019 and currently she is an associate professor. Her field of research is on Artificial Intelligence (AI) and Image Processing. Most of her publications are published in various AI related journals and she has been awarded with several local research grants in Malaysia. She is actively involved with multi discipline research studying AI applications in medical imaging, language and agriculture.



zhen, China.

Professor Hong Zhang received his B.S. from Northeastern University (Boston) in 1982, and Ph.D. from Purdue University in 1986, both in Electrical Engineering. Subsequently he conducted post-doctoral research at the University of Pennsylvania before he joined the Department of Computing Science at the University of Alberta, Canada, where he worked for over 30 years. Since October 2020, he has been a Chair Professor in the Department of Electronic and Electrical Engineering at the Southern University of Science and Technology in Shen-